J. Fluid Mech. (1975), *vol.* 68, *part* 1, *pp.* 41–48
Printed in Great Britain

Instability of a periodic boundary layer in a stratified fluid

By R. M. ROBINSON AND A. D. McEWAN
CSIRO, Division of Atmospheric Physics, Aspendale, Victoria 3195, Australia

(Received 3 December 1973 and in revised form 17 June 1974)

It has been found that the periodic boundary layer formed on a vertically oscillating vertical wall bounding a stratified fluid is liable to two distinct modes of wavelike instability. In the first, which arises when the oscillation frequency ω is lower than 0·7 times the buoyancy frequency N, the phase lines are aligned horizontally. The second mode, in which the phase lines are aligned at 45° or more to the horizontal, becomes dominant as ω is increased above $0{\cdot}9N$.

In distinction from the unstratified periodic Stokes layer, there appears to be, for ω in the vicinity of N, a definite low threshold to the boundary-layer Stokes–Reynolds number (defined as $W_0/(2\omega\nu)^{\frac{1}{2}}$, where W_0 is the maximum vertical wall velocity and ν is the kinematic viscosity) above which the instability is sustained at a detectable level.

1. Introduction

There is considerable literature on the stability of time-dependent viscous shear flows in a homogeneous fluid. Among these studies are Collins (1963), Conrad & Criminale (1965) and Grosch & Salwen (1968) to mention but a few. Of relevance to the present work are the studies of von Kerczek (1973) and von Kerczek & Davis (1974). These authors carried out both quasi-steady and 'exact' linear analyses on the stability of the classical Stokes-layer flow, which is the flow induced in a semi-infinite body of constant-density fluid by a plate of infinite extent oscillating harmonically in is own plane. The quasi-steady theory gave a critical Stokes–Reynolds number $W_0/(2\nu\omega)^{\frac{1}{2}}$† of 43 or 91 depending on the definition of instability while the exact theory predicted stability at least up to a Stokes–Reynolds number of 400. Here W_0 is the velocity amplitude of the oscillating plate, ν is the kinematic viscosity and ω is the angular frequency. Available experimental evidence, referred to by von Kerczek & Davis (1974), seems to indicate a critical Stokes–Reynolds number of about 250.

Very little has been reported on the stability of time-dependent boundary layers in stratified fluids. Hart (1971) has examined experimentally the stability of a stratified fluid bounded by a sloping plane surface oscillating in its own plane. He observed the formation of evenly spaced convective plumes and suggested that they were associated with density-gradient reversals produced by the boundary-layer flow.

† Their definition of 'Reynolds number' is twice ours, i.e., $(2W_0^2/\nu\omega)^{\frac{1}{2}}$.

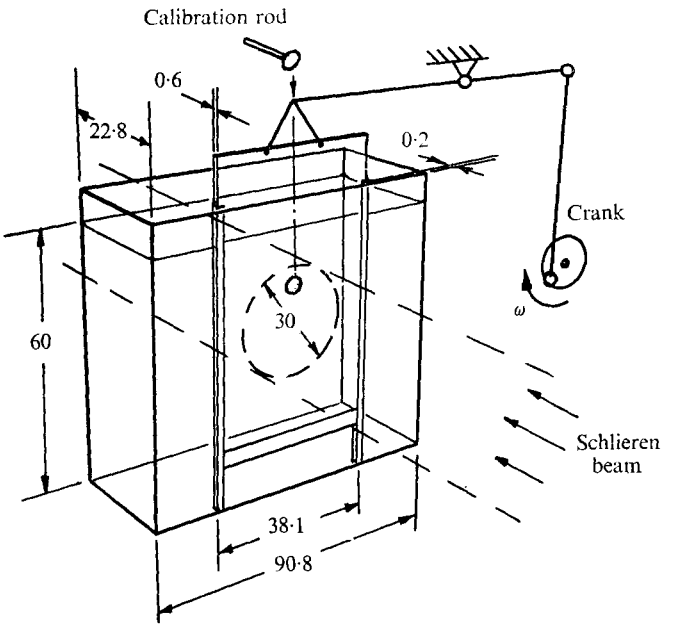

FIGURE 1. Experimental arrangement. Dimensions in cm.

This note describes the results of an experiment designed to examine the instability of the periodic boundary flow produced by a vertical surface oscillating vertically in its own plane and bounding a density-stratified fluid. By using a sensitive schlieren system aligned at right angles to the oscillating surface (made of glass) it is observed that there are two distinct modes of instability, each producing its own quite regular wave pattern. One of the wave patterns has horizontal phase lines parallel to the oscillating plate and will be called 'horizontal waves', while the other has its phase lines parallel to the glass plate but at a distinct angle to the horizontal and will be called 'oblique waves'. Interest in these phenomena arose from the observation of these boundary-layer instabilities when large amplitude internal waves were generated in a vertically sided testing tank.

2. Experimental details

Reference is made to figure 1. The experiments were carried out in a rectangular glass tank of length 90·8 cm, width 22·8 cm and height 68·6 cm filled to 60 cm. Two plastic tracks were glued to one inside glass wall such that a plane glass sheet 38·1 cm wide, 77·5 cm deep and 0·6 cm thick could be positioned by the tracks and could be oscillated vertically in its own plane. The glass sheet, when in position, was 2 mm from the wall of the tank, a distance small enough to maintain parallel flow. The upper end of the glass sheet was connected to a d.c. motor in such a way as to give a vertical displacement sinusoidal in time. The displacement amplitude and period could be varied continuously. Edge-generated turbulence was minimized by fairing the lower edge of the plate.

Common salt in water was used to produce a uniform linear density gradient whose buoyancy frequency was in the range $2\pi/10{\cdot}2$–$2\pi/7{\cdot}46$ s^{-1} for various experiments. To find the buoyancy frequency of the fluid a horizontal round cylinder of diameter 9·5 mm was attached normal to the glass sheet, which was oscillated with a frequency ω. By measuring the angle θ between the emitted waves and the horizontal, the buoyancy frequency could be calculated from the formula

$$N = \omega/\sin\theta$$

(see Mowbray & Rarity 1967).

Visual observation of instabilities in the boundary-layer flow was achieved by the use of a 12 in. (30·5 cm) f8 schlieren system aligned normal to the plane of the oscillating glass plate. The image of a horizontal knife edge was refocused at an occluding horizontal edge to maximize the sensitivity of the visualization to vertical gradients of density. Resolution was estimated to be $3{\cdot}5\times10^{-5}$ (gm cc^{-1} cm^{-1}) cm^{-1} along the light path.

3. The boundary-layer flow

Suppose that the fluid system of the experiment in the central region of the oscillating glass sheet can be approximated by that of a stratified fluid with undisturbed density $\rho_0 = \rho_0^*(1-\beta z)$ occupying the half-space $x > 0$ bounded by a vertical wall at $x = 0$ moving with a vertical velocity $W_0\sin\omega t$. Then to the Boussinesq approximation the basic boundary layer produced by the oscillating wall is described by the equations

$$\left.\begin{aligned} \rho_0^*\,\partial W/\partial t &= -g\rho_1 + \rho_0^*\,\nu\,\partial^2 W/\partial x^2, \\ \partial\rho_1/\partial t + W\,d\rho_0/dz &= 0, \\ W = W_0\sin\omega t \quad \text{at} \quad x = 0, \quad W \to 0 \quad \text{as} \quad x &\to \infty, \end{aligned}\right\} \tag{1}$$

where ρ_1 is the departure of the density from its undisturbed value, ν the kinematic viscosity, g the gravitational acceleration and x and z the horizontal and vertical space co-ordinates. Diffusion in the density equation has been neglected because the Prandtl number ν/κ ($\kappa \equiv$ coefficient of salt diffusion) is large, of order 10^3, and the boundary layer due to salt diffusion has very little effect on the much thicker viscous boundary layer. The solution to (1) is

$$\left.\begin{aligned} W &= W_0\exp(-kx)\sin(\omega t + \operatorname{sgn}(N-\omega)\,kx), \\ \rho_1 &= (-\rho_0^*\beta W_0/\omega)\exp(-kx)\cos(\omega t + \operatorname{sgn}(N-\omega)\,kx), \end{aligned}\right\} \tag{2}$$

where $k = [(\omega/2\nu)\,|N^2/\omega^2 - 1|]^{\frac{1}{2}}$. Here $N = (\beta g)^{\frac{1}{2}}$ is the buoyancy frequency. No attempt was made to measure the accuracy of this description but obviously when N^2/ω^2 is near 1 the finite extent of the container will restrain the thickness of the boundary layer, although (2) predicts that it will become infinite at $N^2/\omega^2 = 1$. In the limit of vanishing density gradient $\beta \to 0$, the flow represented by (2) reduces to the classical Stokes-layer flow.

Leaving aside the constraints imposed by the container, the motion is characterized completely by two dimensionless quantities: the Stokes–Reynolds number $R = W_0/(2\nu\omega)^{\frac{1}{2}}$ and the frequency ratio ω/N.

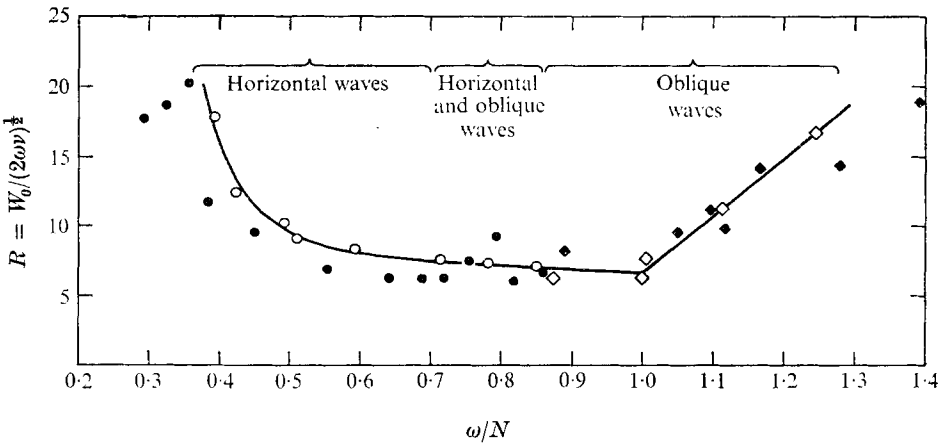

FIGURE 2. Critical Stokes–Reynolds number as a function of the frequency. ○, $N = 2\pi/7{\cdot}46\ \mathrm{s}^{-1}$, horizontal wave limit; ◇, $N = 2\pi/7{\cdot}46\ \mathrm{s}^{-1}$, oblique wave limit; ●, $N = 2\pi/10{\cdot}1\ \mathrm{s}^{-1}$, horizontal wave limit; ◆, $N = 2\pi/10{\cdot}1\ \mathrm{s}^{-1}$, oblique wave limit. The solid line is a subjectively fitted curve.

4. Experimental results

Two distinct modes of instability were observed, one giving rise to horizontal waves and the other producing waves with phase lines at an angle to the horizontal. A striking feature of the disturbances was their regularity, both in space and time, at Stokes–Reynolds numbers slightly above the critical values.

4.1. *Critical Stokes–Reynolds number*

The critical value R_c of R is shown in figure 2 for various values of ω/N when $N = 2\pi/7{\cdot}46\ \mathrm{s}^{-1}$ and $N = 2\pi/10{\cdot}1\ \mathrm{s}^{-1}$. The temperature of the salt solution was 21 °C and the kinematic viscosity in R was taken as $0{\cdot}01\ \mathrm{cm}^2\ \mathrm{s}^{-1}$. Critical values were found by first forcing at high amplitude till the disturbance was plainly visible in the schlieren image and then very carefully and slowly reducing the amplitude until it was barely discernible but had not completely disappeared. The sharp rate at which the disturbance weakened with small decreases in amplitude gave confidence in the accuracy of this technique. The size of the amplitudes examined was restricted by the intrusion of turbulence, generated at the edges, into the region of viewing. On figure 2 open and closed symbols are used to identify results from the separate experiments with different density gradients. Limiting modes of instability are denoted by differently shaped symbols.

In the set with the open symbols ($N = 2\pi/7{\cdot}46\ \mathrm{s}^{-1}$) the lowering of the oscillation amplitude was very gradual, and the scatter is correspondingly small. The solid symbols, from an earlier set with $N = 2\pi/10{\cdot}1\ \mathrm{s}^{-1}$, give a slightly lower R_c over most of the range. This discrepancy may have arisen partly from the difficulty in discriminating between waves and a weak residual layering beyond the boundary layer, evidently associated with the boundary instability.

In both cases the minimum R_c was about 6, and occurred with ω/N near unity. R_c increased only gradually as ω was reduced until ω/N was about 0·5, after which the increase was more rapid. For $\omega/N > 1{\cdot}0$ the increase in R_c was nearly linear. The solid line on the figure has been subjectively fitted to the open symbols.

4.2. *Oblique waves*

Oblique waves occurred for frequencies near the natural frequency of the fluid. For values of ω/N in the approximate range (0·87, 1·3) only oblique waves were ever observed. In the approximate range (0·7, 0·87) horizontal waves were the first to appear but for sufficiently large forcing amplitudes these would evolve into oblique waves. The horizontal wave mode reappeared if the amplitude was slowly reduced. Figure 3 (plate 1) is a photograph taken during the transition from the horizontal mode to the oblique mode. The oblique mode could exist either with just one set of parallel-crested waves or with both positive and negative angles to form a hatched or cellular pattern. For $\omega/N \lesssim 0{\cdot}7$ only the horizontal mode was observed and increasing the forcing amplitude would only cause the regular horizontal waves to become distorted and eventually lead to mixing. Figure 4 (plate 1) illustrates a purely horizontal mode.

The angle of the crests of the oblique waves to the horizontal was observed to vary with both the Stokes–Reynolds number and the frequency. With R just above the critical value for the oblique waves, and with the frequency in the mixed-mode range, i.e. $0{\cdot}7 < \omega/N < 0{\cdot}87$, the angles were observed to be close to the angle $\theta = \sin^{-1}(\omega/N)$, the characteristic angle of internal waves at that frequency. For higher R the hatched pattern became distorted; the angles varied in space and time and were generally smaller than at critical values but were never observed to be less than 45° (which is the lowest value of $\theta = \sin^{-1}(\omega/N)$ in the mixed-mode range). Throughout the oblique-mode range, i.e. $0{\cdot}87 \lesssim \omega/N \lesssim 1{\cdot}3$, the angles were approximately 60° (the highest value of $\theta = \sin^{-1}\omega/N$ in the mixed-mode range). Figures 5 and 6 (plate 2) illustrate the oblique modes with $\omega/N = 1{\cdot}25$ and 1·0 respectively. In both cases

$$N = 2\pi/7{\cdot}46 \text{ s}^{-1}$$

and the amplitude is just greater than critical. Figure 7 (plate 3) shows the large amplitude development of an oblique mode. With the forcing maintained the pattern became increasingly turbulent. Figures 3–7 are photographs of the schlieren image and reveal an elevation view of the density-gradient variations integrated through the fluid in the direction normal to the oscillating plate. The dark background squares are formed by a 10×10 cm reference grid fixed on the test tank. The additional line in figures 4–6 is drawn on the oscillating plate and shows the vertical displacement of the plate from the central horizontal line.

4.3. *Dominant wavelengths*

Figure 8 gives the average values of the dominant horizontal (λ_w) and vertical (λ_v) wavelength of the waves, as derived from photographs taken during the experiments that gave the results in figure 2. These wavelengths are non-dimensionalized by a factor $\omega^{\frac{1}{2}}\nu^{-\frac{1}{2}}$ and plotted against ω/N. It will be seen that

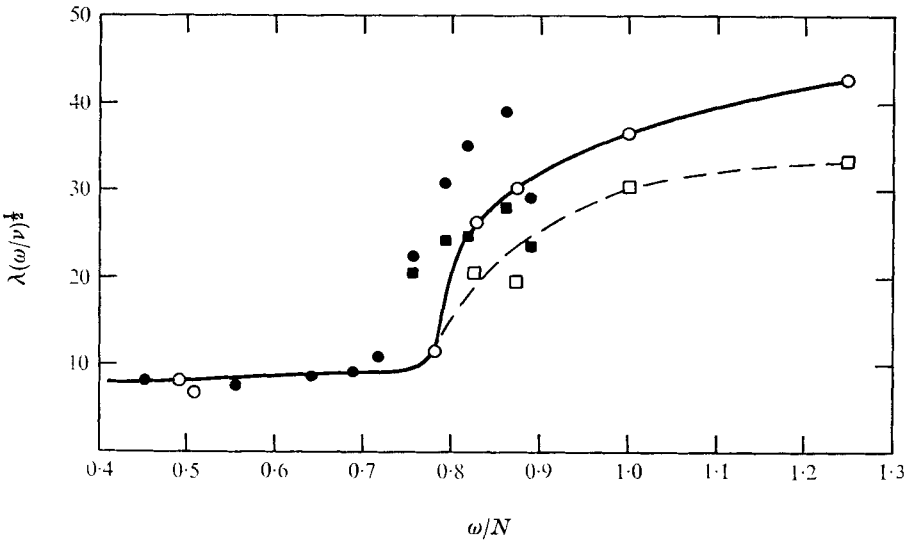

FIGURE 8. Dominant wavelengths of observed instability. Solid symbols, $N = 2\pi/10{\cdot}1\ \mathrm{s}^{-1}$; open symbols, $N = 2\pi/7{\cdot}46\ \mathrm{s}^{-1}$. ●, ○, vertical wavelength λ_v; ■, □, horizontal wavelength λ_h.

in the horizontal wave regime λ_v remained more or less constant but rose abruptly as the mixed, horizontal–oblique wave regime was entered. The horizontal wavelength of the oblique waves rose less rapidly, consistent with an increasing characteristic angle θ.

The vague resemblance of figures 8 and 2 suggests that the wavelength might be dependent on R. A particular dependence which eliminated ν would not be surprising since, as pointed out by a referee, a vertical scale h can be derived from balance between viscous and buoyancy forces, giving $h = W_0 |N^2 - \omega^2)|/N^2\omega$. Correlations of the form $\lambda(\omega/\nu)^{\frac{1}{2}} = f(\omega/N)\, g(R)$ were attempted but no consistent relation could be found, and the misalignment in ω/N between the two experiments is unaccounted for.

4.4. *Periodic history*

The amplitude and phase velocity of the disturbance waves varied through a period of oscillation. In the lower frequency range $\omega/N \lesssim 0{\cdot}87$ and for R not too far above critical the evolution of horizontal and oblique waves could be clearly followed. On the upward stroke the disturbance became visible just before the top of the stroke at $\omega t = 0$ and had a slow downward phase velocity†, which continually decreased with time. The disturbance amplitude, determined by the degree of contrast in the schlieren image between crests and troughs, reached a maximum at about $\omega t = \frac{1}{4}\pi$, after which it decreased and became no longer visible at about $\omega t = \frac{1}{2}\pi$, i.e. at zero displacement of the oscillating wall; see (2). The evolution was repeated in a similar manner during the other half of the

† The phase velocity is defined here as the apparent vertical propagation speed of horizontal lines of maximum density contrast, as revealed and measured using frame-by-frame analysis of cinema records of the schlieren image.

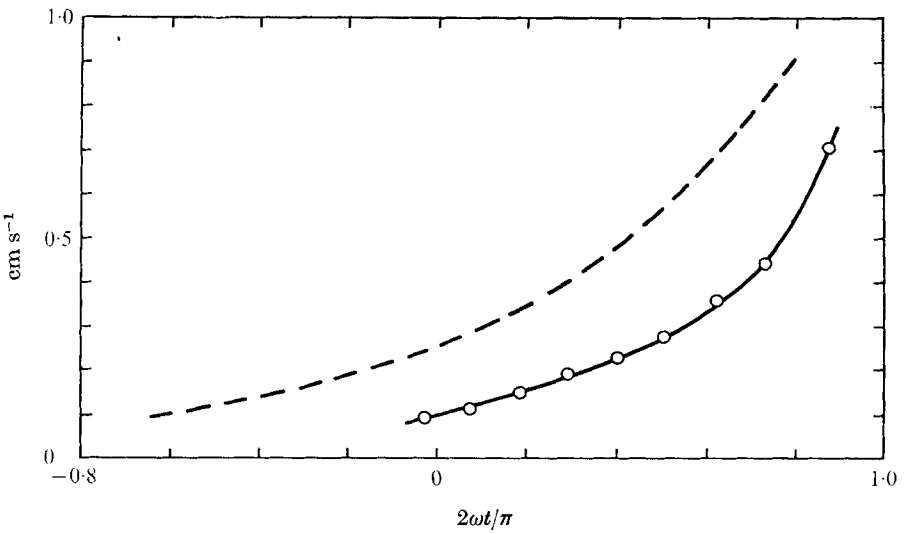

FIGURE 9. The measured phase velocity (circles) and instantaneous velocity of main point inflexion (dashed line) of horizontal waves as functions of time for the situation $N = 2\pi/10{\cdot}1\ \mathrm{s}^{-1}$, $R = 13{\cdot}7$, $\omega/N = 0{\cdot}66$.

stroke from $\omega t = \frac{1}{2}\pi$ to $\omega t = \frac{3}{2}\pi$. Figure 9 illustrates the phase velocity measured from movie films of the experiment for a particular situation in which the disturbances were horizontal waves. Also indicated is the z-wise velocity of particles of fluid occupying the instantaneous point of inflexion [i.e. $W(x(W_{xx} = 0), t)$] as given by (2). It can be seen that the measured phase velocity is less than, but has a qualitative similarity to the velocity of the instantaneous point of inflexion. This implies that the disturbances were embedded in the boundary layer and were advected to some degree by the flow.

In distinction, waves for the upper frequency range $\omega/N \gtrsim 0{\cdot}87$ appeared to be standing waves, and showed very little translation. They seemed to remain stationary and change phase smoothly without discernable periods of obvious growth and decay, especially for frequencies above the buoyancy frequency. Their disinclination to be advected, regardless of oscillation amplitude, suggested that they lay mainly outside the boundary layer.

5. Concluding remarks

We have experimentally studied the stability of the boundary layer on a vertically oscillating vertical plane wall in a stratified fluid. Two modes of instability were observed and their occurrence depended on the frequency and amplitude of the oscillation. For frequency ratios ω/N in the approximate ranges $(0{\cdot}3, 0{\cdot}7)$, $(0{\cdot}7, 0{\cdot}87)$ and $(0{\cdot}87, 1{\cdot}3)$ the observed modes of instability were, respectively, horizontal waves, horizontal waves becoming oblique waves at a higher amplitude and oblique waves. The critical Stokes–Reynolds number increased for frequencies away from the natural frequency (figure 2).

In the horizontal wave regime, the vertical wavelength remained at about $9(\nu/\omega)^{\frac{1}{2}}$ almost independently of the frequency. For oblique waves both the horizontal and vertical wavelengths increased from this value, steeply at first, as the oscillation frequency was increased.

Calculations show the total energy in the flow (kinetic plus potential) for the case $\omega < N$ in a half-period to be a maximum at $\omega t = -\frac{1}{8}\pi$ and a minimum at $\omega t = \frac{3}{8}\pi$, approximately the period during which disturbances are observed (see §4.4). Thus, if a decreasing total energy is associated with a decelerating flow then disturbances are observed during the decelerating part of the flow. For $\omega > N$ the total energy is a maximum at $\omega t = -\frac{3}{8}\pi$ and a minimum at $\omega t = \frac{1}{8}\pi$ but, as pointed out in §4.4, there is no obvious period of growth observed for this frequency range.

A comprehensive, numerical, quasi-steady, linear stability analysis, not reported here, was carried out in an attempt to describe the observed phenomena. It was found to describe some features of the horizontal mode of instability. In particular it predicted quite accurately the observed wavelengths and gave positive growth rates during observed growth periods. The analysis proved to be completely inadequate in predicting the observed oblique mode. A possible explanation for this is that the oblique waves are a consequence of a resonant coupling between the oblique mode and the basic flow and that this resonance cannot be detected simply by considering a quasi-steady system. Tentatively then, it would seem that the horizontal mode is essentially a consequence of the basic flow profile, with regard of course to the density stratification, while the oblique mode is a consequence of the periodic nature of the boundary-layer flow. A definitive examination of this view awaits a full time-dependent analysis such as that carried out by von Kerczek & Davis (1974) for the homogeneous case.

REFERENCES

COLLINS, J. I. 1963 Inception of turbulence at the bed under periodic gravity waves. *J. Geophys. Res.* **68**, 6007.

CONRAD, P. W. & CRIMINALE, W. O. 1965 The stability of time-dependent laminar flow: parallel flows. *Z. angew. Math. Phys.* **16**, 233.

GROSCH, C. E. & SALWEN, H. 1968 Stability of steady and time-dependent plane Poiseuille flow. *J. Fluid Mech.* **34**, 177.

HART, J. E. 1971 A possible mechanism for boundary layer mixing and layer formation in a stratified fluid. *J. Phys. Oceanog.* **1**, 258.

KERCZEK, C. VON 1973 On the stability of Stokes layers. Ph.D. thesis, Dept. Mech. & Materials Sci., The Johns Hopkins University.

KERCZEK, C. VON & DAVIS, S. H. 1974 Linear stability theory of oscillatory Stokes layers. *J. Fluid Mech.* **62**, 753.

MOWBRAY, D. E. & RARITY, B. S. H. 1967 A theoretical and experimental investigation of the phase configuration of internal waves of small amplitude in a density stratified liquid. *J. Fluid Mech.* **28**, 1.

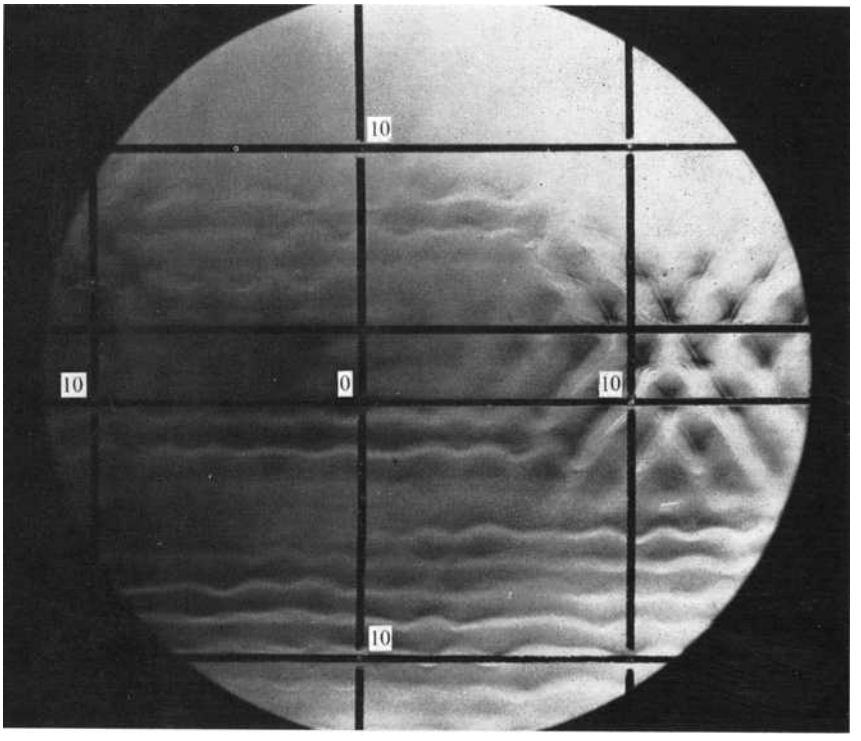

FIGURE 3. A view facing the vertically oscillating plate showing a transition from the horizontal mode to the oblique mode. $N = 2\pi/7{\cdot}46\ \mathrm{s}^{-1}$, $\omega/N = 0{\cdot}87$.

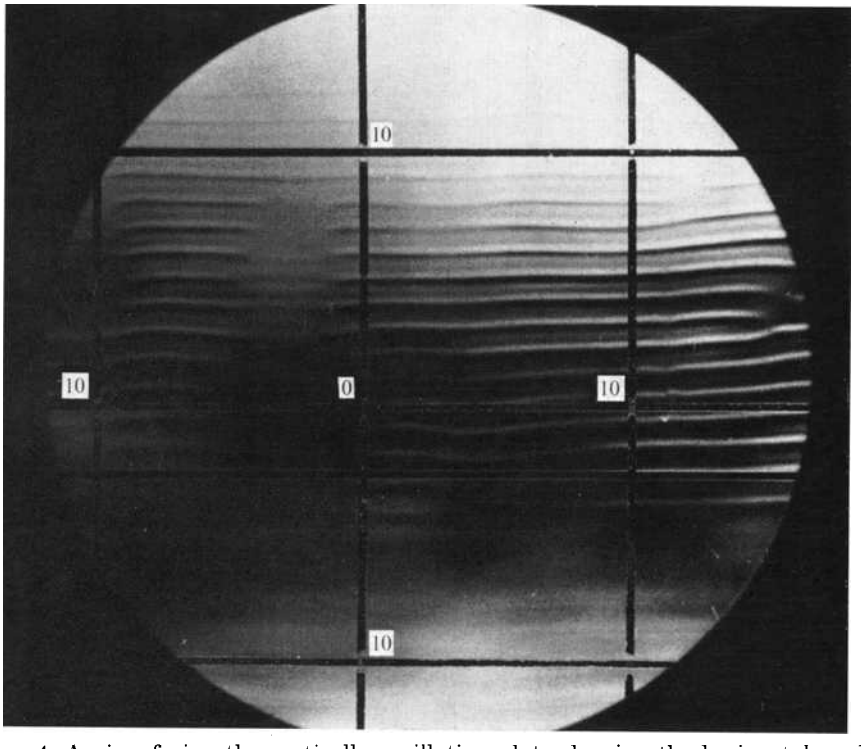

FIGURE 4. A view facing the vertically oscillating plate showing the horizontal mode of instability. $N = 2\pi/7{\cdot}46\ \mathrm{s}^{-1}$, $\omega/N = 0{\cdot}51$.

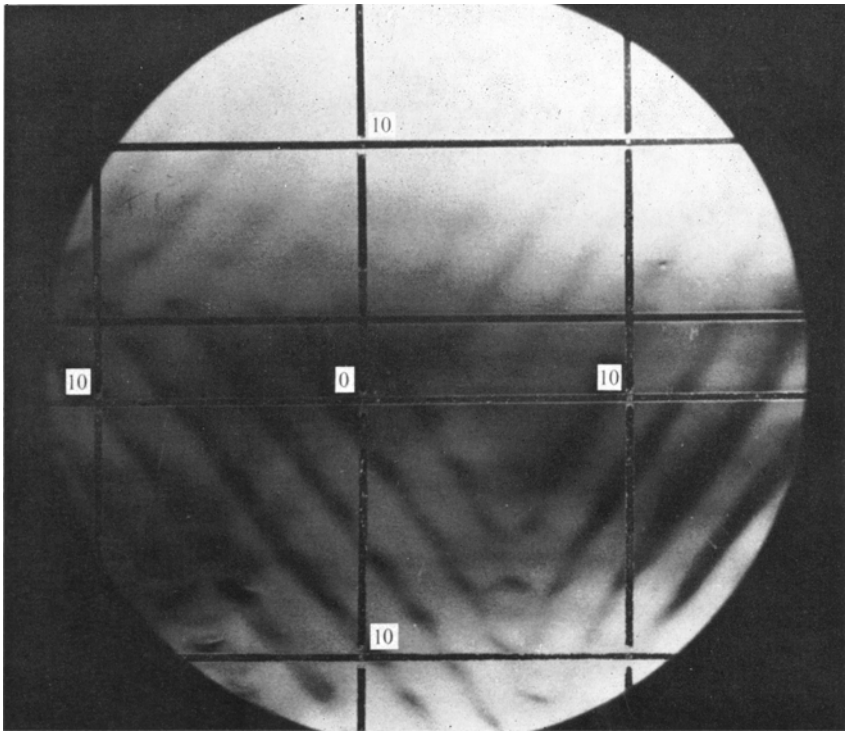

FIGURE 5. A view facing the vertically oscillating plate showing the oblique mode of instability. $N = 2\pi/7{\cdot}46\ \mathrm{s}^{-1}$, $\omega/N = 1{\cdot}25$.

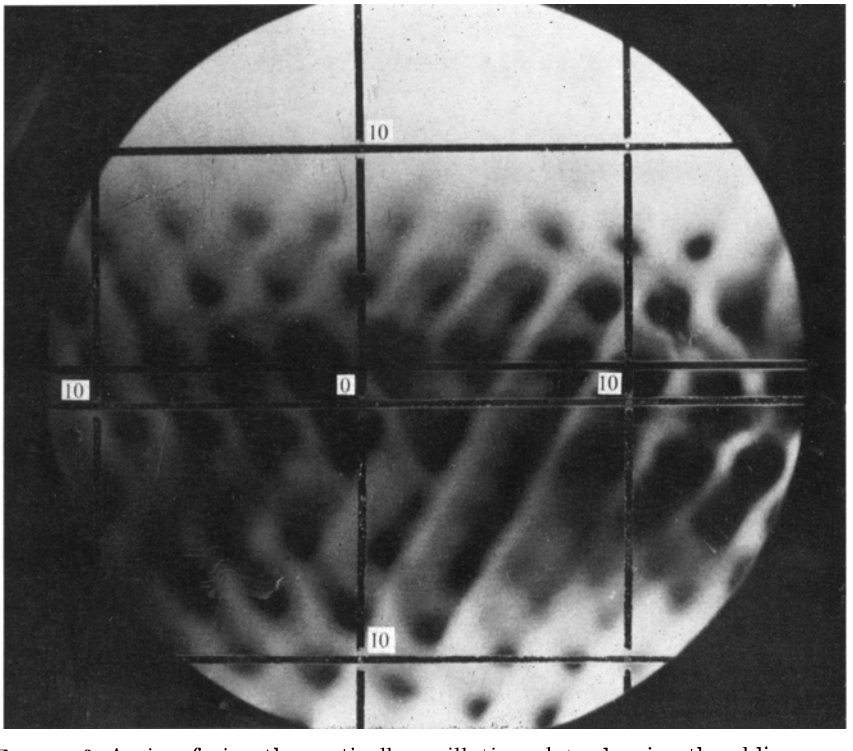

FIGURE 6. A view facing the vertically oscillating plate showing the oblique mode of instability. $N = 2\pi/7{\cdot}46\ \mathrm{s}^{-1}$, $\omega/N = 1{\cdot}0$.

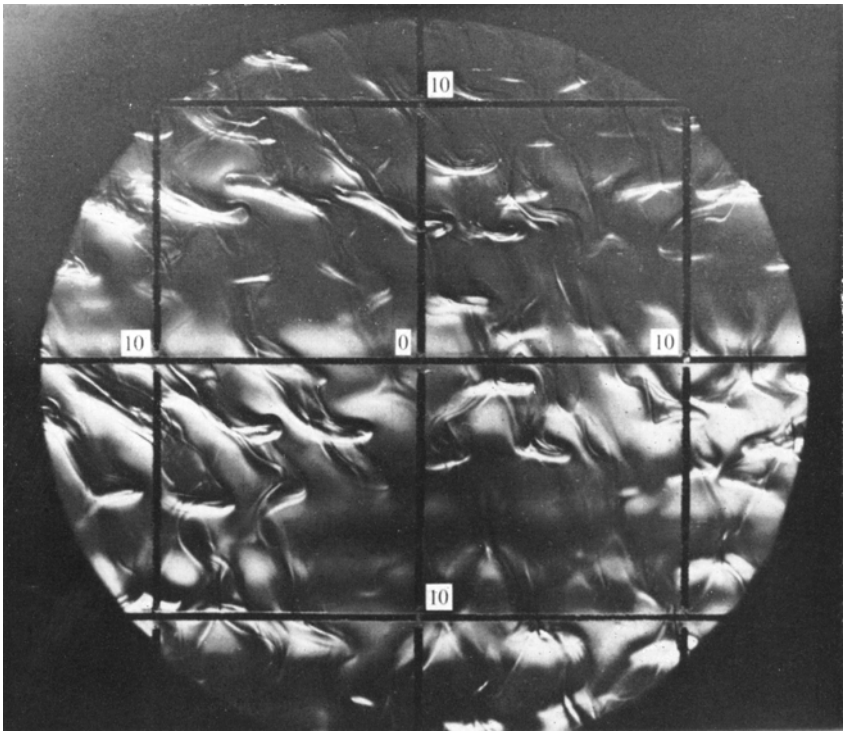

FIGURE 7. A view facing the vertically oscillating plate showing the large amplitude development of an oblique wave.